RSC Advances

ROYAL SOCIETY OF CHEMISTRY

www.rsc.org/advances

Journal Name

ARTICLE

Enhanced catalytic performance of a Pt-xCeO_2/Graphene catalyst for DMFCs by adjusting the crystal-plane and shape of nanoscale ceria

Received 00th January 20xx,
Accepted 00th January 20xx

DOI: 10.1039/x0xx00000x

www.rsc.org/

Weihua Wang[a], Mingda Zhu[a], Xiaolin Lu[a], Yanfang Gao*[a], Lijun Li*[1a], Zhenzhu Cao[a], Caihong Li[a], Jinrong Liu[a], Haitao Zheng[b]

Oxygen storage capacity is influenced by the morphology and crystal-plane(s) of CeO_2, which can thus affect the ability of this material to oxidise carbon monoxide. To investigate the effect of different morphologies/crystal-planes of CeO_2 on the electrocatalytic performance of DMFCs（Direct Methanol Fuel cell），three different types of CeO_2 nanocrystals with different crystal-planes were synthesised and later assembled into Pt-xCeO_2/Graphene composites with graphene and Pt nanoparticles as the electrocatalyst for DMFCs. According to the HRTEM images, the original morphology and crystal-plane structures of CeO_2 are essentially maintained in the three types of Pt-xCeO_2/Graphene composite catalysts investigated in this work. The catalytic performance of the Pt-xCeO_2/Graphene composites for methanol electrocatalytic oxidation was investigated by a series of electrochemical measurements. Compared with the other catalysts, Pt-rCeO_2/Graphene demonstrates superior catalytic activity (onset potential: 0.15 V) and the strongest resistance to poisoning by carbonaceous species (I_f/I_b: 2.11). The results of H_2-TPR shows that rCeO_2 with the {110} facet has the best surface reducibility among the xCeO_2 with different facets being investigated, which provides a rationale for the superior performance of the Pt-rCeO_2/Graphene catalyst. This study indicates that metallic oxides with a suitable crystal plane and shape can effectively enhance the electrocatalytic performance of Pt-based catalysts for methanol electrooxidation.

Introduction

Because of their high energy density, low operating cost, compact design, and reliance on a liquid fuel (methanol), direct methanol fuel cells (DMFCs) exhibit great promise for practical application in transportation and portable devices.[1] Pt-based catalysts, which are the best catalysts in anodic electrocatalysis of DMFCs[2], have been limited by their low utilization and high cost[3]. Moreover, these catalysts are easily poisoned by reaction intermediates such as carbon monoxide[4]. To overcome such defects, efforts have been devoted to developing Pt-based alloys such as Pt-Ru, Pt-Ni, Pt-Au, etc. for use as catalysts.[5] Additionally, researchers have found that metal oxides can efficiently promote electrocatalytic and anti-poisoning properties of Pt-based catalysts. In this context, Pt-based metal oxides composites, such as Pt/CeO_2, Pt/MnO_2, Pt/Fe_2O_3, and Pt/TiO_2[6, 7] have been shown to improve the electrocatalytic performance of Pt-based nanoparticles while demonstrating significant tolerance to CO poisoning. Among the metal oxides, CeO_2 is of particular interest because of its high activity during the oxidation of carbon monoxide[8, 9]. Recently, Chu *et al.*[10] reported that the composite derived from loading Pt/CeO_2 onto a carbon-based material showed high activity for methanol electrooxidation and significant tolerance to CO poisoning.

In previous research[6, 8-10], all of the Pt-CeO_2/carbon-based materials were optimized to achieve the greatest electrocatalytic activity either by i) tuning the scale of CeO_2 in the composite material, ii) changing the carbon-based supports, or iii) improving the dispersion of Pt nanoparticles. In fact, because of its incredible physicochemical properties such as high surface area, sizable surface defects, and high oxygen storage capacity (i.e., Ce^{4+}/Ce^{3+} redox sites)[11], the presence of ceria in Pt/CeO_2-based composites mostly acts as a promoter that improves the oxidation of CO to CO_2 via the lattice oxygen species[12]. This unique redox property is usually described in terms of a material's oxygen storage capacity (OSC) [11-13].

[a] College of Chemical Engineering, Inner Mongolia University of Technology, Hohhot, P. R. China.
[b] Materials Science and Manufacturing, Council for Scientific and Industrial Research (CSIR).
*E-mail: yf_gao@imut.edu.cn（Gao Yanfang），lilijun@imut.edu.cn（Li Lijun）.
Electronic Supplementary Information (ESI) available, See
DOI: 10.1039/x0xx00000x

It is well known that the redox features of ceria as described by its OSC are largely influenced by its morphology and depends on the exposed crystal plane.[13] Ceria with different morphologies and crystal-planes will exhibit different reducibilities, which could profoundly affect its capacity to oxidize carbon monoxide[14-16]. For example, Si *et* al.[14] studied the shape and crystal-plane effects of nanoscale ceria on the activity of Au-CeO_2 catalysts for the water-gas shift reaction and found that the rod-shaped CeO_2 enclosed by the {110} and {100} planes were the most active for carbon monoxide oxidation. In this context, a designed surface morphology/crystal plane CeO_2 with high reducibility is especially important for improving the activity and durability of catalysts for DMFCs.

Owing to its unique properties such as a high surface area and high electrical conductance, graphene (G) is an attractive material to be used as a conductive support in DMFCs.[8, 9, 17] Here, we have successfully synthesised three types of CeO_2 nanocrystals with different morphologies/lattice planes: rod-shaped CeO_2 nanocrystals with the {110} and {100} crystal planes, cube-shaped CeO_2 nanocrystals with the {100} crystal plane, and polyhedron-shaped CeO_2 nanocrystals with the {111} and {100} crystal planes). The nanocrystals are assembled with graphene and Pt nanoparticles to form the Pt-$xCeO_2$/G composite catalyst, where $xCeO_2$ indicates the shape of the cerium oxide species. Specifically, $rCeO_2$ indicates a rod-shaped CeO_2, $cCeO_2$ indicates a cube-shaped CeO_2, and $pCeO_2$ indicates a polyhedra-shaped CeO_2. The composite catalyst were used to investigate the effect(s) of the different morphologies/lattice planes of CeO_2 on the electrocatalytic properties of DMFCs. The results indicate that the rod-shaped CeO_2 enclosed by the {110} and {100} facets can greatly enhance the catalyst's activity for methanol electrooxidation. Moreover, relative to the other CeO2 species investigated, rod-shaped CeO_2 has a higher resistance to poisoning by carbonaceous species, which we attribute to a higher concentration of oxygen vacancies on the CeO_2 {110} facet.

Experimental Section

Material

All chemicals were of analytical grade and used as received without further purification. Potassium permanganate ($KMnO_4$), phosphoric acid (H_3PO_4), sulfuric acid (H_2SO_4), absolute ethanol (C_2H_5OH), sodium hydroxide (NaOH) and ethylene glycol (EG) were purchased from Tianjing Chemical Reagents Limited Cooperation (Tianjing, China). Cerium (III) nitrate hexahydrate ($Ce(NO_3)_3{\cdot}6H_2O$), hydrogen peroxide (H_2O_2) and Nafion® were purchased from Sinopharm Chemical Reagent Limited Cooperation. Other reagents were purchased from Aladdin Industrial Corporation.

Synthesis of graphene oxide

Graphene oxide (GO) was synthesised by a slightly modified Hummers method.[38] Briefly, 3.0 g of flake graphite was added to a 9:1 mixture of H_2SO_4/H_3PO_4 (360/40 mL). Then, 18.0 g of $KMnO_4$ was added to the above solution while stirring. The reaction was then heated to 50℃ and stirred for 20 hours (h). Once the solution was cooled to room temperature it was poured onto ice (approximately 400 mL). A 30% H_2O_2 solution was then added dropwise into the cooled solution until the colour tuned brown. The obtained product was collected by centrifugation, washed repeatedly with deionized water and ethanol and dried in vacuum at 60℃ for 10 h.

Synthesis of different shaped CeO_2 nanoparticles

Schematic diagram for the shape-selective synthesis of CeO2 nanopolyhedra, nanocubes and nanorods was shown in Fig. S1. The synthesis of rod-shaped CeO_2 followed the procedure of Mai *et al*.[28] Briefly, $Ce(NO_3)_3{\cdot}6H_2O$ (1.736 g) was dissolved in deionized water (40 mL), and in another solution NaOH (19.2 g) was also dissolved in deionized water (40 mL). Then, these two solutions were mixed in a Teflon bottle and stirred for 30 min at room temperature until a milky slurry was formed. Subsequently, the Teflon bottle was tightly sealed and hydrothermally treated in a stainless-steel autoclave at 100℃ for 24 h. After cooling, the obtained white precipitate was collected by centrifugation, washed with deionized water, and dried at 60℃ in air overnight. The synthetic procedure for cube-shaped CeO_2 was similar to the synthesis the rod-shaped CeO_2 except that the hydrothermal treatment temperature was set to 180℃. Likewise, the synthetic procedure for polyhedra-shaped CeO_2 was identical to that employed for rod-shaped CeO_2 except that the weight of NaOH was 0.32 g.

Synthesis of the Pt-$xCeO_2$/Graphene catalyst

30 mg of the obtained $xCeO_2$, 60 mg of graphene oxide and 20 mg of polyvinyl pyrrolidone（PVP） was dispersed into 18 mL of distilled water and ultrasonicated for 0.5 h. Then, 2 mL of 0.05 M aqueous solution of chloroplatinic acid (H_2PtCl_6) was added, stirred for 1 h, and then 60 mg of $NaBH_4$ was added. After the mixture was stirred for 2 h, it was then heated to 60℃ and stirred for an additional 30 min. After the mixture was cooled to room temperature, the obtained product (i.e., the Pt-$xCeO_2$/Graphene electrocatalyst) was collected by centrifugation, washed with deionized water, and dried at 60℃ in air overnight. The synthetic procedure is shown in Scheme 1.

< **Scheme1** >

Scheme1. Schematic synthetic protocol for Pt-$rCeO_2$/Graphene, Pt-$cCeO_2$/Graphene, Pt-$pCeO_2$/Graphene composite materials.

Characterisations

The morphology and structure of the samples were investigated by field emission SEM (FESEM, Hitachi S-3400N) and high-resolution TEM (HRTEM, FEI Tecnai G20 microscope

operated at 200 kV), and the energy dispersive X-ray (EDS) spectrogram was recorded from the same FESEM. The powder X-ray diffraction (XRD; Brucker, D8-Advance) with Cu-Kα radiation (λ=0.15406 nm) was used to characterise the composition and crystal structure of the samples. The H_2-TPR experiment was performed using a Micromeritics Chemisorb 2750 TPD/TPR system. Typically, 50 mg of $xCeO_2$ was loaded into a U-shaped quartz tube. After pre-treatment for 1 h at 250℃ in a flowing 20% O_2/N_2 mixture (25 mL/min), the samples were cooled to room temperature under flowing N_2. The samples were then heated to 850℃ at a rate of 10℃·min^{-1} under a flowing 5% H_2/N_2 mixture (20 mL/min).

Electrochemical characterisation and measurements

Cyclic voltammetric and chronoamperometric measurements were performed on a CHI 660 electrochemical workstation (CH Instruments, Austin, TX) in a standard three-electrode cell that used a platinum wire as the counter electrode and an Ag/AgCl electrode as the reference electrode. The working electrode was prepared as follows: 2.5 mg of Pt-$xCeO_2$/Graphene catalyst was dispersed in a mixture of 0.5 mL ethanol and 7.5μL Nafion®. After ultrasonication for 30 minutes, 5.0μL of the suspension was transferred to a glass carbon (*GC*) electrode surface, which was polished with Al_2O_3 by a microsyringe. The *GC* electrode was then dried in air at room temperature.

The cyclic voltammogram (*CV*) experiments for hydrogen absorption/desorption were performed in a 1 M N_2-saturated H_2SO_4 aqueous solution. The potential was cycled from -0.25 to 1.25 V at a scan rate of 50 mV/s. The *CVs* for CH_3OH oxidation were performed in a mixture of N_2-saturated 0.5 M H_2SO_4 and 0.5 M CH_3OH. Here, the potential was cycled from 0 to 1 V at a scan rate of 50 mV/s. The chronoamperometric curves were recorded for 1000s at a fixed voltage of 0.7 V in the same 0.5 M H_2SO_4 and 0.5 M CH_3OH mixed solution.

Results and Discussion

To obtain cerium oxide with different morphologies/crystal-planes, we used a simple hydrothermal method for its synthesis. The hydrothermal process obeys the so-called dissolution/recrystallisation mechanism[15, 18], such that different types of cerium oxide can be obtained by adjusting the hydrothermal temperature and concentration of NaOH. As seen from the TEM and high-resolution TEM (HRTEM) images shown in Figure 1, $rCeO_2$, $cCeO_2$, and $pCeO_2$ all possess uniform morphologies. In Figure 1a and 1d, the rod-shaped CeO_2 has a diameter of *ca.* 12 nm and a length distribution between 50 and 300 nm. Figure 1d shows two interplanar spacings of 0.198 nm and 0.269 nm, which indicate the (220) and (200) planes. This configuration reflects the rod-shaped CeO_2 enclosed by the {110} and {100} facets, as Figure 1g shown. From the other images in Figure 1, the cube-shaped CeO_2 shows an edge length distribution between 20 nm and 50 nm, and the polyhedra-shaped CeO_2 shows a diameter of *ca.* 10 nm. Two interplanar spacing at 0.274 nm and 0.279 nm can be observed from Figure 1e, which indicate the (200) planes of $cCeO_2$. This configuration reflects that only the {100} facet is enclosed on the cube-shaped CeO_2, as shown in Figure 1h. Finally, Figure 1f shows interplanar spacings of 0.278 nm, 0.311 nm and 0.316 nm, which indicate that the polyhedra-shaped CeO_2 is enclosed by the {111} and {100} facets, as shown in Figure 1i. The further verification of the formation of cerium oxide with different morphologies/crystal-planes can be conducted with the help of XRD analysis (see Fig. S2).

< **Figure 1** >

Figure 1. TEM and HRTEM images of rod-shaped CeO_2 (a, d), cube-shaped CeO_2 (b, e), and polyhedra-shaped CeO_2 (c, f). The schematics of rod-shaped CeO_2, cube-shaped CeO_2, and polyhedra-shaped CeO_2 are shown in (g), (h), and (i), respectively.

According to the literature, [12, 19] the reducibility of CeO_2 is greatly enhanced by surface defects such as oxygen vacancies, the exposure of suitable facets, and large surface areas. CeO_2 exposed to different crystal planes also affects the amount and density of surface oxygen vacancies. Thus, the preferential exposure of CeO_2 to appropriate facets could greatly enhance the reducibility of CeO_2. In this regard, we characterised H_2-TPR to compare the reducibility between differently shaped CeO_2.

< **Figure 2** >

Figure 2. H_2-TPR of rod-shaped CeO_2, cube-shaped CeO_2, and polyhedra-shaped CeO_2.

Figure 2 shows the H_2-TPR of rod-shaped CeO_2, cube-shaped CeO_2, and polyhedra-shaped CeO_2. The low temperature peak (below 600℃) is caused by the reduction of the surface capping oxygens and the high temperature area (above 600℃) is caused by the reduction of bulk oxygen.[20, 21] The low-temperature area of the CeO_2 reduction profile indicates that this material is a better catalyst for low-temperature oxidation reactions.[12] The initial surface reduction temperature represents the surface reducibility. From Figure 2, rod-shaped CeO_2 have the lowest initial surface reduction temperature (approximately 200℃). Cube-shaped CeO_2 and polyhedra-shaped CeO_2 (approximately 275℃) have similar starting temperatures (approximately 280℃ and 275℃, respectively). In the curve of rod-shaped CeO_2, the low temperature reduction peak area is significantly larger than the other reduction peak areas. This can be attributed to the presence of a larger number and higher density of surface oxygen vacancies, as well as a large number of reactive oxygen species on the surface of the rod-shaped CeO_2.[12, 20] This result suggests that rod-shaped CeO_2 have the best surface reducibility among the differently shaped CeO_2 catalysts investigated.

As we have demonstrated in our H_2-TPR experiment, rod-shaped CeO_2 have the best surface reducibility. Mai *et al.*[14] and Si *et al.*[15] have investigated the oxygen storage behaviour of ceria with different crystal-planes and shapes and found that

rod-shaped CeO_2 with surface structures dominated by {110} and {100} facets are more reactive towards CO oxidation than CeO_2 shaped differently. These groups indicated that this result could be attributed to the higher concentration of oxygen vacancies of CeO_2 on the {110} facet.

Figure 3a shows the morphology of the Pt-rCeO_2/Graphene composite. As seen, a distinct crinkled structure of the graphene can be observed. Figure 3b is a typical EDS spectrum of Pt-rCeO_2/Graphene, which corresponds to the data in Figure 3a. The data reveal that the mass fractions of Pt and rCeO_2 are 17.39% and 28.76%, respectively. Notably, these values are essentially consistent with our initial design. XRD patterns of graphene oxide (GO), rCeO2/RGO, Pt-rCeO2/Graphene composites were shown in Fig. S3.

< **Figure 3** >

Figure 3. SEM of Pt-rCeO_2/Graphene (a) and the EDS spectrum of (b) Pt-rCeO_2/Graphene corresponding to (a); HRTEM images of Pt-rCeO_2/Graphene (c), Pt-cCeO_2/Graphene (d), and Pt-pCeO_2/Graphene (e).

In Figures 3c–e, although the edge of xCeO_2 is imperfect, the original morphology of xCeO_2 is fairly well maintained in the Pt-xCeO_2/Graphene composite catalyst, with some scattered Pt nanoparticles in the vicinity. In addition, Figure 3c shows that the rCeO_2 in the Pt-rCeO_2/Graphene composite is enclosed by the {110} and {100} facets. Similarly, Figures 3d–e show that xCeO_2 in the Pt-cCeO_2/Graphene composite is enclosed by the {100} facet and is enclosed by the {111} and {100} facets in the Pt-pCeO_2/Graphene composite. The more detailed verification can be conducted with the (TEM) (see Fig. S4).

The cyclic voltammograms of Pt-rCeO_2/G, Pt-pCeO_2/G, Pt-cCeO_2/G, and Pt/G in a 0.5 M H_2SO_4 solution at scan rates of 50 mV/s are shown in Figure 4. Two hydrogen (H_2) adsorption/desorption peaks between -0.15 and 0.2 V (*vs.* Ag/AgCl) can be clearly discerned. The electrochemically active surface areas (ESA) of the catalysts are calculated from the following equation: [8, 22]

$$\mathrm{ESA}\ (m^2 g^{-1}) = \frac{Q_H}{2.1 \times [\mathrm{Pt}]}$$

Here, Q_H represents the charge of H_2 desorption, and [Pt] represent the quantity of Pt that is loaded on the electrode. Table 1 shows the calculated results for the ESA of Pt for Pt-rCeO_2/G (62.6 m^2/g), Pt-cCeO_2/G (59.2 m^2/g), Pt-pCeO_2/G (65.8 m^2/g) and Pt/G (56.1 m^2/g). The ESA of the Pt-xCeO_2/Graphene catalysts do not differ significantly from the calculated results (from 59.2 m^2/g to 65.8 m^2/g). This suggests that there was little difference in the extent of Pt dispersion between the different Pt-xCeO_2/G catalysts. We note that the ESA of Pt/G (56.1 m^2/g) gives the lowest value. Overall, the results suggest that the dispersion of Pt does not significantly influence the electrochemical performance of the different Pt-xCeO_2/G catalysts.

To investigate the electrochemical performance of the catalysts by doping with differently shaped CeO_2, we have recorded the cyclic voltammograms of Pt-rCeO_2/G, Pt-pCeO_2/G, Pt-cCeO_2/G, and Pt/G in 0.5 M H_2SO_4+0.5 M CH_3OH solutions at scan rates of 50 mV/s. The corresponding data are summarised in Table 1. The catalytic performance of methanol electrooxidation can be described by the forward scanning peak current density (I_f) and the onset potential of the cyclic voltammograms curves. As seen in Table 1, Pt-rCeO_2/G and Pt-pCeO_2/G show relatively high forward scanning peak current densities of 286.7 mA/mg and 284.4 mA/mg, respectively. The analogous value for Pt-cCeO_2/G is only 235.6 mA/mg. We note that Pt-rCeO_2/G gives an ultra-low onset potential of 0.152 V; however, Pt-pCeO_2/G and Pt-cCeO_2/G give onset potentials of 0.186 V and 0.21 V, respectively. These results suggest that Pt-rCeO_2/G has superior catalytic activity for methanol electrooxidation relative to the other catalysts investigated.

< **Figure 5** >

Figure 5. Cyclic voltammograms of Pt-rCeO_2/G, Pt-pCeO_2/G, Pt-cCeO_2/G, and Pt/G in mixed solutions of 0.5 M H_2SO_4 with 0.5 M CH_3OH at scan rates of 50 mV/s.

Table 1. Data corresponding to the results from the cyclic voltammetry experiments.

< **Table 1** >

According to the literature[9, 23], a high ratio of the forward anodic peak current density (I_f) to the backward anodic peak current density (I_b), I_f/I_b, implies that the catalyst has a stronger tolerance to carbonaceous species formed during the anodic electrooxidation of methanol. From Table 1, Pt-rCeO_2/G has the highest I_f/I_b ratio (of 2.11) compared to the other materials, which indicates that the Pt-rCeO_2/G composite has the highest tolerance to carbonaceous species. We note that the ratios (I_f/I_b) of Pt-pCeO_2/G (1.71) and Pt-cCeO_2/G (1.73) are very similar. These results are consistent with the results from the H_2-TPR experiments that showed rCeO_2 ({110}, {100}) to possess the best surface reducibility, whereas the surface reducibility of cCeO_2 ({100}) and pCeO_2 ({100}, {111}) are similar. As seen In Figure 6, the Pt-rCeO_2/G and Pt-pCeO_2/G composites clearly have higher forward scanning peak current densities than the Pt-cCeO_2/G and Pt/G composites (see also Table 1). These results suggest that the rod-shaped CeO_2 enclosed by the {110}, {100} facets can more effectively promote the performed of the catalyst for methanol electrooxidation than the cube-shaped CeO_2 enclosed by the {100} facet or the polyhedra-shaped CeO_2 enclosed by the {111}, {100} facets. Moreover, the rod-shaped CeO_2 can greatly enhance the catalyst's resistance to poisoning by carbonaceous species.

< **Figure 6** >

Figure 6. Chronoamperometry curves of Pt-rCeO_2/G, Pt-pCeO_2/G, Pt-cCeO_2/G, and Pt/G in mixed solutions of 0.5 M H_2SO_4 + 0.5 M CH_3OH at 0.7 V for 1000s.

Chronoamperometric curves are usually employed to evaluate the activity and stability of a catalyst. Figure 6 shows the chronoamperometry curves of Pt-rCeO_2/G, Pt-pCeO_2/G, Pt-cCeO_2/G, and Pt/G in mixed solutions of 0.5 M H_2SO_4 + 0.5 M CH_3OH at 0.7 V for 1000 s. Because of poisoning caused by carbonaceous species such as CO_{ads} and CHO_{ads}, all of the curves for each catalyst shown in Figure 6 display a sharp drop at the outset of the experiment. Compared with cube-shaped CeO_2, the activities of the catalysts doped by rod-shaped CeO_2 and polyhedra-shaped CeO_2 decrease rather gradually. After 1000 s of continual measurements, the current density of the Pt-rCeO_2/G catalyst retains an I_f/I_b ratio that is approximately 3.0, 2.1, 2.0 times higher than the Pt/G, Pt-cCeO_2/G, and Pt-pCeO_2/G catalysts, respectively. These results clearly indicate that rCeO_2 can promote a higher activity and stability to the catalyst than either cCeO_2 or pCeO_2.

Collectively, the data indicate that rod-shaped CeO_2 enclosed by the {110} and {100} facets can more effectively enhance the catalyst's activity and resistance to poisoning by carbonaceous species for DMFCs than either cube-shaped CeO_2 enclosed by the {100} facets or polyhedra-shaped CeO_2 enclosed by the {111} and {100} facets. The results of calculations using simulated amorphisation and recrystallisation (A&R) [24] suggest that the formation energies for oxygen vacancies follows the order {110}<{100}<{111}, which implies that oxygen vacancies are easier to form for rCeO_2 enclosed by the {110} and {100} facets. Because the {100} facet is a polar surface[14], the concentration of oxygen vacancies for cCeO_2 is as low as pCeO_2, which is enclosed by the {111} and {100} facets. For this reason, rCeO_2 shows more reactivity towards CO oxidation than either pCeO_2 or cCeO_2. Further, pCeO_2 shows similar reactivity to cCeO_2, even though it has been reported that pCeO_2 shows higher reactivity.[14, 15]

This works describes the first attempt to determine the performance of the Pt-xCeO_2/Graphene catalyst for methanol electrooxidation. The performance of the catalyst can be optimised by tuning the crystal planes and shape of the metallic oxide species. The results presented herein provide new insights for developing highly efficient electrocatalysts with superior anti-poisoning capabilities for use in DMFCs.

Conclusions

We successfully synthesised three different types of cerium oxides with different shapes in this work. According to HRTEM images, rod-shaped CeO_2 are enclosed by {110} and {100} facets, cube-shaped CeO_2 are enclosed by {100} facets, and polyhedra-shaped CeO_2 are enclosed by {111} and {100} facets. We assembled the CeO_2 species with graphene and Pt nanoparticles into Pt-xCeO_2/Graphene composite materials for use as an electrocatalyst for DMFCs. In the HRTEM image of the Pt-xCeO_2/Graphene composite catalysts, the original morphology and facets of xCeO_2 are essentially maintained. H_2-TPR was used to monitor the oxygen storage capacity of the differently shaped CeO_2. The results from these investigations indicated that rod-shaped CeO_2 have the best surface reducibility and that cube-shaped and polyhedra-shaped CeO_2 have nearly identical surface reducibilities. A series of electrochemical measurements were performed to characterize the performance of the Pt-xCeO_2/Graphene catalyst towards methanol electrooxidation. The results demonstrate that rod-shaped CeO_2 enclosed by the {110} and {100} facets could greatly enhance the catalyst's activity for methanol electrooxidation. Further, rod-shaped CeO_2 impart the catalyst with superior resistance to poisoning by carbonaceous species. In contrast, Pt-cCeO_2/G and Pt-pCeO_2/G are more susceptible to such poisoning.

Overall, the results provide clear evidence that CeO_2 with suitable crystal planes can greatly improve the electrocatalytic performance of Pt-based catalysts for methanol electrooxidation.

Acknowledgments

This work was financially supported by the National Natural Science Foundation of China (No.21266018), the Science and Technology projects of Science and Technology Department of Inner Mongolia Autonomous Region, P. R. China (No.20110401 and No.20130409), the Natural Science Foundation of Inner Mongolia, P. R. China (No.2010MS0218), the Program for Young Talents of Science and Technology in the Universities of Inner Mongolia Autonomous Region (No. NJYT-15-A04), the Ministry of Science and Technology China-South Africa Joint Research Program (No.CS08-L15) and the National Research Foundation (South Africa, CHN14033166025).

Notes and references

1 *(a)* A. Lam, D. P. Wilkinson and J. J. Zhang, *J. Power Sources*, 2009,194 , 991-996; *(b)* V. D. Noto, E. Negro, R. Gliubizzi, S. Lavina, G. Pace, S. Gross and C. Maccato, *Adv. Funct. Mater*, 2007, 17, 3626-3638; *(c)* M. K. Jeon, J. Y. Won, K. R. Lee, S. I. Woo, *Electrochemistry Communications*, 2007, 9, 2163-2166; *(d)* E. H. Yu, X. Wang, U. Krewer, L. Li, K. Scott, *Energy Environ Sci*, 2012, 5, 5668-5680.

2 *(a)* X. Ren, M. S. Wilson, S. Gottesfeld, *J. Electrochem. Soc*. 1996 ,143, L12-L14; *(b)* E. N. Coker, W. A. Steen, J. T. Miller, A. J. Kropfc and J. E. Miller, *J. Mater. Chem*, 2007, 17, 3330-3340; *(c)* E. Antolini, *Energy Environ. Sci*, 2009, 2, 915-931.

3 *(a)* L. Kuai, S. Wang and B. Geng, *Chem. Commun*, 2011, 47, 6093-6095; *(b)* L. Kuai, B. Geng, S. Wang and Y. Sang, *Chem. Eur. J*, 2012, 18, 9423-9429; *(c)* L. Feng, X. Zhao, J. Yang, W. Xing and C. Liu, *Catalysis Communications*, 2011,14, 10-14.

4 *(a)* S. Liao, K. A. Holmes, H. Tsaprailis and V. I. Birss, *J. Am. Chem. Soc*, 2006, 128, 3504-3505; *(b)* T. Cochell, A. Manthiram, *Langmuir*, 2012, 28, 1579-1587.

5 *(a)* Z. Jiang, Z. Jiang, *Electrochimica Acta*, 2011, 56, 8662-8673; *(b)* P. Piela, C. Eickes, E. Brosha, F. Garzon and P. Zelenay, *J. Electrochem. Soc*, 2004, 151, A2053-A2059; *(c)* T. C. Deivaraj, W. X. Chen, J. Y. Lee, *J Mater Chem*, 2003,13 , 2555-2560; *(d)* J. Wang, G. Yin, H. Liu, R. Li, R. L. Flemming and X. Sun, *Journal of Power Sources*, 2009,194, 668-673.

6 Y. Zhou, Y. Gao, Y. Liu and J. Liu, *Journal of Power Sources*, 2010,195, 1605-1609.

7 *(a)* C. Zhou, H. Wang, F. Peng, J. Liang, H. Yu and J. Yang, *Langmuir*, 2009, 25, 7711-7717; *(b)* V. M. Dhavale, S. Kurungot, *Journal of Physical Chemistry C*, 2012, 116, 7318-7326; *(c)* S. Y. Huang, P. Ganesan, S. Park and B. N. Popov, *J. Am. Chem. Soc*, 2009, 131, 13898-13899.

8 S. Yu, Q. Liu, W. Yang, K. Han, Z. Wang and H. Zhu, *Electrochimica Acta*, 2013, 94, 245-251.

9 X. Wang, X. Li, D. Liu, S. Song and H. Zhang, *Chem.Commun*, 2012, 48, 2885-2887.

10 Y. Y. Chu, J. Cao, Z. Dai and X. Y. Tan, *J. Mater. Chem. A*, 2014, 2, 4038-4044.

11 A. Trovarelli, *Catal. Rev. Sci. Eng*. 1996, 38, 439-520.

12 S. K. Meher, G. R. Rao, *ACS Catal*, 2012, 2, 2795-2809.

13 Tana, M. Zhang, J. Li, H. Li, Y. Li and W. Shen, *Catalysis Today*, 2009, 148, 179-183.

14 R. Si, M. F. Stephanopoulos, *Angew. Chem. Int. Ed*, 2008, 47, 2884-2887.

15 H. X. Mai, L. D. Sun, Y. W. Zhang, R. Si, W. Feng, H. P. Zhang, H. C. Liu and C. H. Yan, *J. Phys. Chem. B*, 2005, 109, 24380-24385.

16 Y. Yamada, C. K. Tsung, W. Huang, Z. Huo, S. E. Habas, T. Soejima, C. E. Aliaga, G. A. Somorjai and P. Yang, *Nature Chemistry*, 2011, 3, 372-376.

17 X. Yu, L. Kuai and B. Geng, *Nanoscale*, 2012, 4, 5738-5743.

18 M. Hirano, E. Kato, *J. Am. Ceram. Soc*. 1999, 82, 786-788.

19 Y. Gao, W. Wang, S. Chang and W. Huang, *ChemCatChem*, 013, 5, 3610-3620.

20 E. Aneggi, M. Boaro, C. Leitenburg, G. Dolcetti and A. Trovarelli, *Journal of Alloys and Compounds*, 2006, 408-412, 1096-1102.

21 G. R. Rao, *Mater. Sci*. 1999, 22, 89-94.

22 H. Zhu, X. Li and F. Wang, *International Journal of Hydrogen Energy*, 2011, 36, 9151-9154.

23 Y. Zhao, L. Zhan, J. Tian, S. Nie, Z. Ning, *Electrochimica Acta*, 2011, 56, 1967-1972.

24 T. X. Sayle, S. C. Parker and D. C. Sayle, *Phys. Chem. Chem. Phys.* 2005, 7, 2936-2941.

25 D. C. Marcano, D. V. Kosynkin, J. M. Berlin, A. Sinitskii, Z. Sun, A. Slesarev, L. B. Alemany, W. Lu and J. M. Tour, *ACS nano*, 2010, 4, 4806-4814.

Scheme1

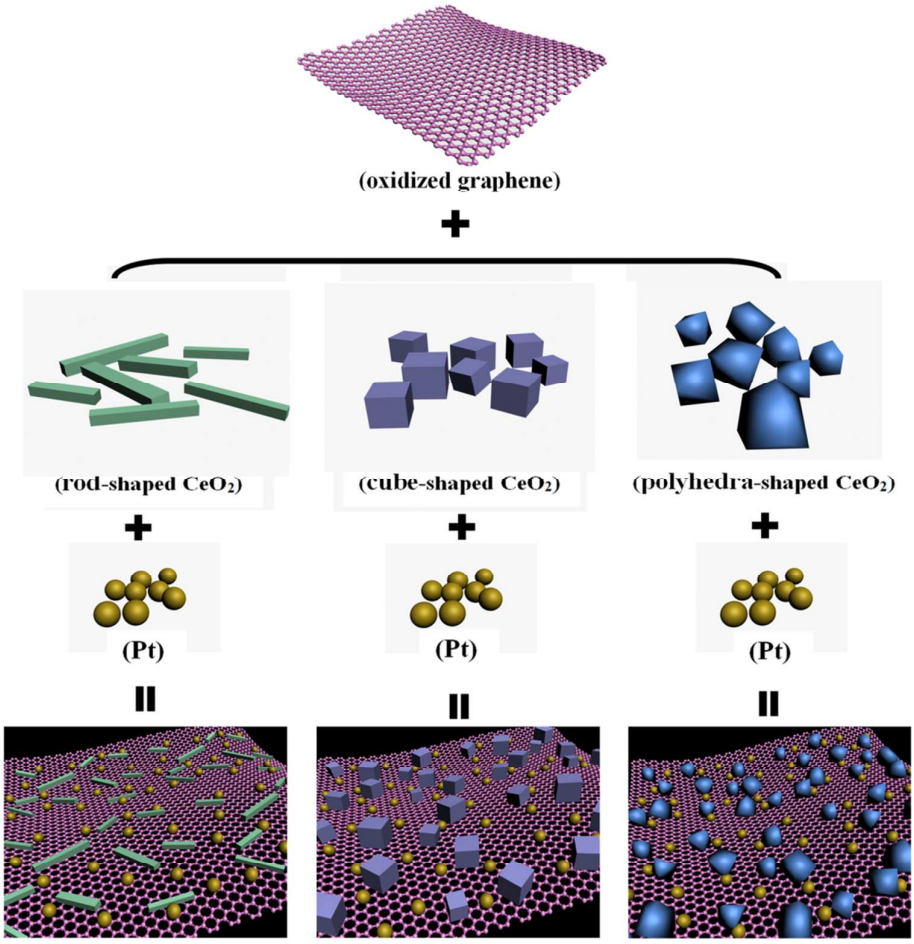

Figure 1

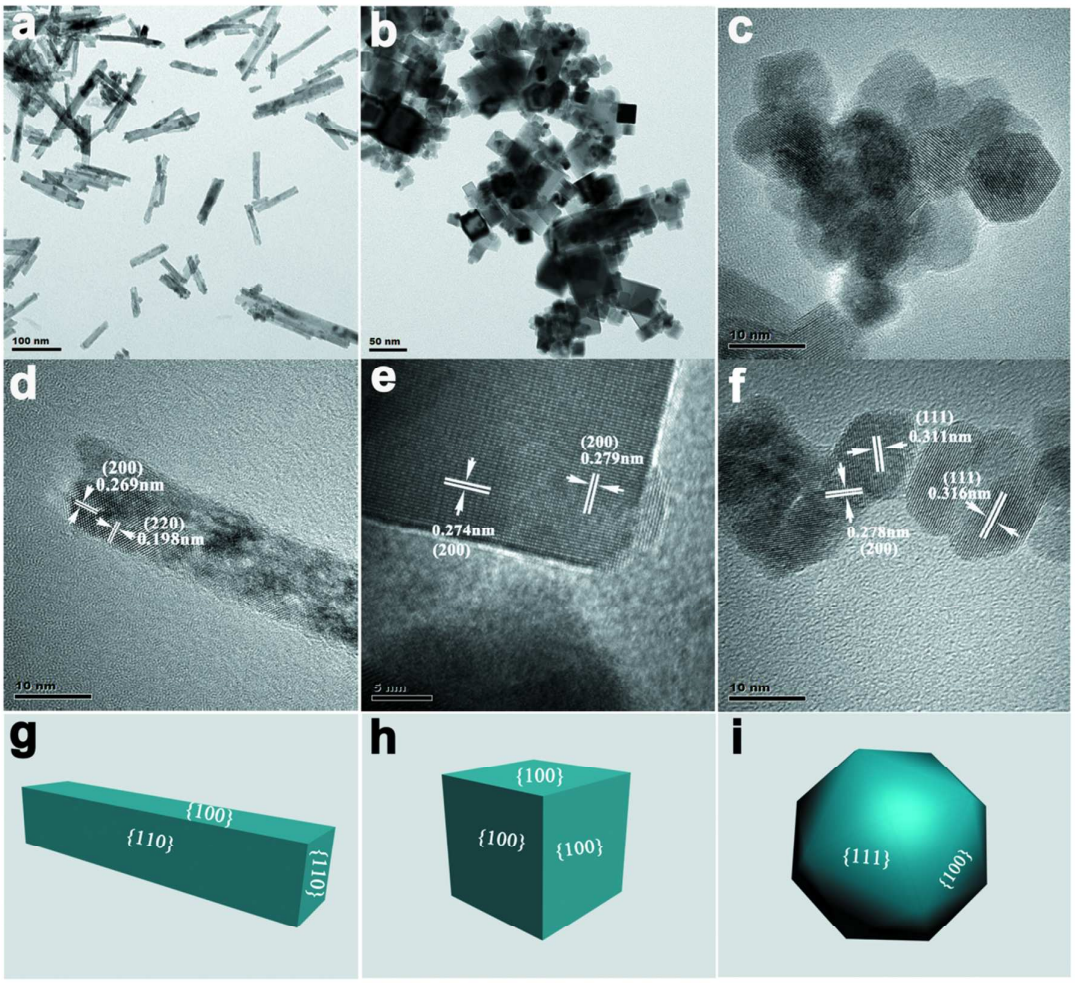

Figure 2

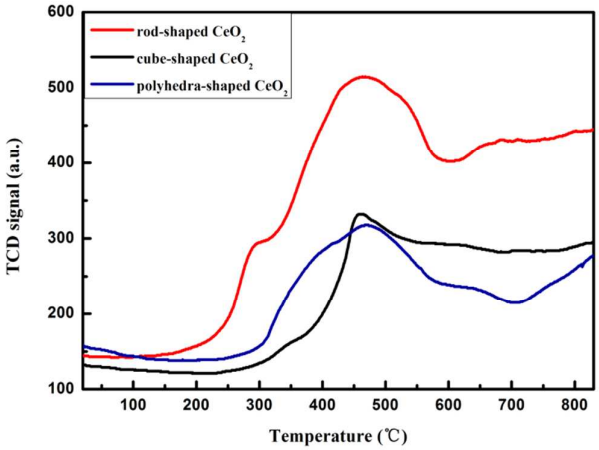

H_2-TPR of rod-shaped CeO_2, cube-shaped CeO_2, and polyhedra-shaped CeO_2.

Figure 3

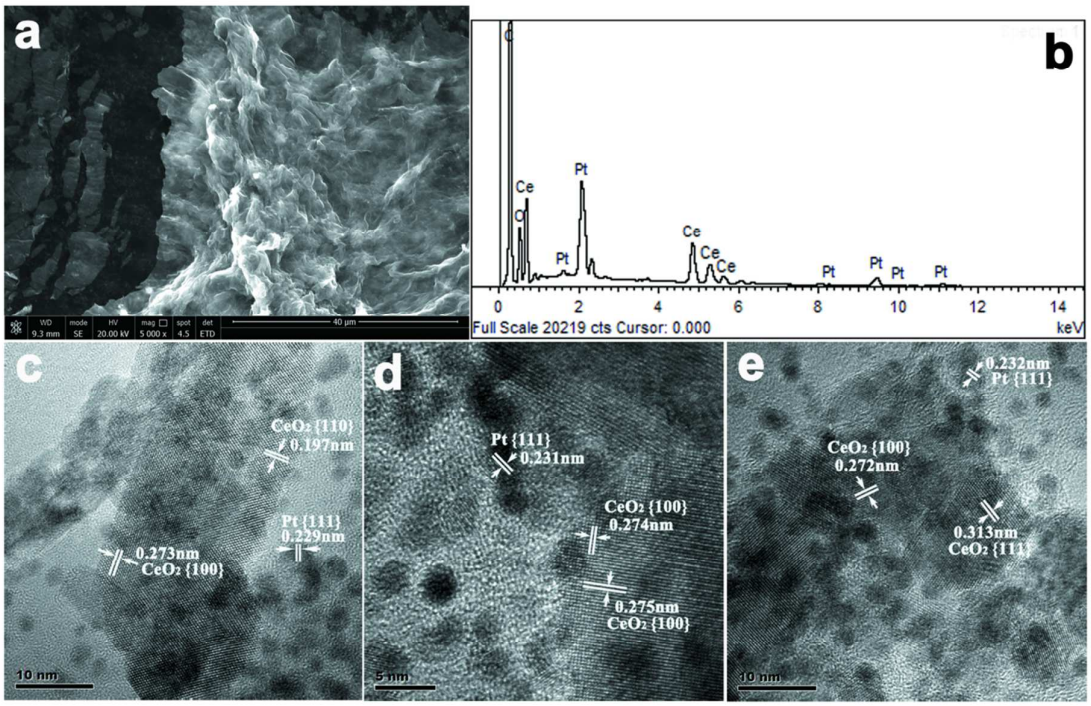

Figure 4

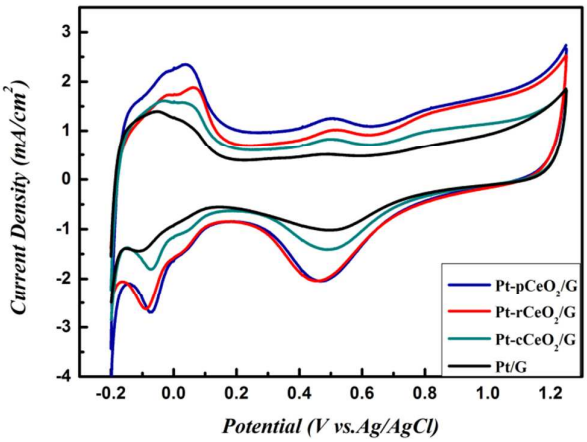

Figure 5

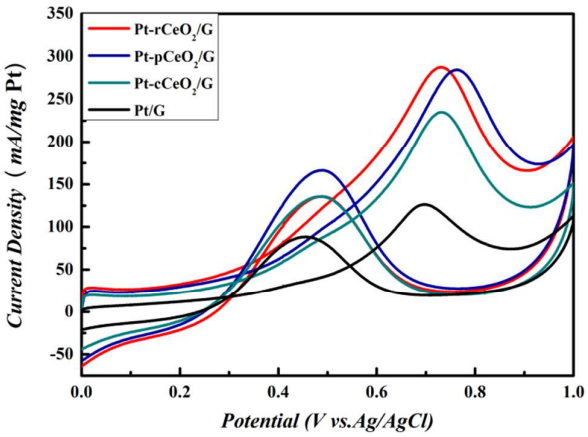

Figure 6

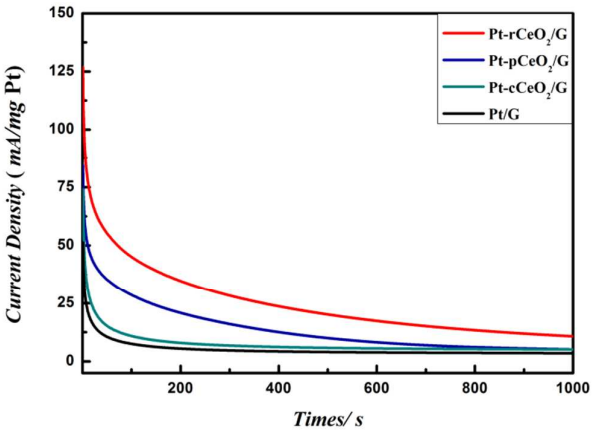

Table 1. the corresponding data of the cyclic voltammograms data.

Catalyst	ESA	Onset potential	I_f peak	I_f	I_f/I_b
Pt-rCeO_2-G	62.6	0.152	0.722	286.7	2.11
Pt-pCeO_2-G	65.8	0.186	0.755	284.4	1.71
Pt-cCeO_2-G	59.2	0.210	0.733	235.6	1.73
Pt-G	56.1	0.216	0.698	126.2	1.43

Graphical Abstract